Applied Catalysis B: Environmental 199 (2016) 166–169

Contents lists available at ScienceDirect

Applied Catalysis B: Environmental

journal homepage: www.elsevier.com/locate/apcatb

# Preparation and photocatalytic activity of triangular pyramid $NaNbO_3$

Qiaonan Yu[a,b], Feng Zhang[a], Guoqiang Li[a,*], Weifeng Zhang[a,*]

[a] Key Laboratory of Photovoltaic Materials of Henan Province, School of Physics & Electronics, Henan University, Kaifeng 475004, PR China
[b] College of Electronics and Electrical Engineering, Nanyang Institute of Technology, Nanyang 473004, PR China

ARTICLE INFO

*Article history:*
Received 16 April 2016
Received in revised form 7 June 2016
Accepted 9 June 2016
Available online 11 June 2016

*Keywords:*
Sodium niobate
Substrate
Triangular pyramid
Photocatalysis

ABSTRACT

The interface will control the morphology, leading to different chemical and physical properties. We obtained $NaNbO_3$ with the morphology of triangular pyramids and cubes on the heterogeneous and homogeneous substrate by hydrothermal method, respectively. In comparison with the cube sample, the triangular pyramid one exhibits higher photocatalytic oxidization activities for 2,4-dichlorophene and rhodamine B degradation under full arc irradiation of Xe lamp. The $^{\bullet}OH$ radical coming from $^{\bullet}O_2^-$ with the intermediate of $H_2O_2$ is identified as the dominant oxide species via various control experiments.

© 2016 Elsevier B.V. All rights reserved.

## 1. Introduction

Semiconductor photocatalysis is an innovative technology, which refers to solar energy conversion and environmental remediation [1,2]. In the past four decades, various semiconductors were examined for the photocatalytic activity, such as water splitting, dye degradation, $CO_2$ reduction and air purification [3,4]. Oxide is a fascinating kind of photocatalysts due to the ease of preparation and stable in air [5,6].

$NaNbO_3$ has an orthorhombic symmetry at room temperature with lattice constants $a_o = 5.569$ Å, $b_o = 5.505$ Å, $c_o = 15.523$ Å, and we also can calculate the pseudocubic lattice parameters of $NaNbO_3$ to $a_c = 3.881$ Å, $b_c = 3.915$ Å, $c_c = 3.915$, and $\alpha_c = 90.67^\circ$ [7,8]. As a photocatalyst, it has the extensive potential applications in solar fuel production and organic pollutant removal [9–16]. Many methods were proposed to improve the activity, such as making solid solution and composites, preparing the nanostructured samples [12,17,18]. From the viewpoint of morphology, nanostructured $NaNbO_3$, such as nanowire, nanocube and nanoplate, were synthesized and investigated for the photocatalytic activity, revealing that the morphology control will bring the enhanced photocatalytic activity [11,12,15,19–21]. Hydrothermal method is a good way to prepare the sample with special morphologies, and free substrate was usual in this method [22,23]. However, some single crystal substrate could be used as the substrate to grow the sample exposed certain facets [24,25]. Moreover, heterogeneous and homogeneous substrates will impact on the morphology of the sample due to the different atomic arrangement of interface. $LaAlO_3$ (a = 3.79 Å) and $SrTiO_3$ (a = 3.80 Å) are often used as the substrate for depositing the pervoskite oxide thin film. $LaAlO_3$ is non-photoactive, whereas $SrTiO_3$ exhibits the good photocatalytic activity. In our previous study, the $NaNbO_3$(111) has the highest activity among the three crystal planes with the low Miller index [26]. Taking consideration of the lattice mismatch and photoactivity into account, we selected the $LaAlO_3$(111) as the heterogeneous substrate, and $NaNbO_3/LaAlO_3$(111) as the homogeneous one.

In this study, we used the heterogeneous and homogeneous substrates to prepare $NaNbO_3$. The triangular pyramids and cubes are obtained on the heterogeneous and homogeneous substrates. They exhibit different photocatalytic oxidization activities for 2, 4-dichlorophene (DCP) and rhodamine B (RhB) degradation under full arc irradiation of Xe lamp. The crystal growth mechanism and detailed oxidization process will be discussed.

## 2. Experimental

Pristine $LaAlO_3$(111) and $NaNbO_3/LaAlO_3$(111) were used as heterogeneous and homogeneous substrates. $NaNbO_3/LaAlO_3$(111) was prepared by pulse laser deposition (PLD) as reported before [26]. $NaNbO_3$ were synthesized via a simple hydrothermal process. Typically, 50 mL of NaOH solution (8 M) and 2 g of $Nb_2O_5$ powder were mixed. The prepared mixture was poured into a 100 mL teflon-lined stainless steel autoclave. The $LaAlO_3$(111) and $NaNbO_3/LaAlO_3$(111) substrates were kept horizontally in the

* Corresponding authors.
*E-mail addresses:* gqli1980@henu.edu.cn (G. Li), wfzhang@henu.edu.cn (W. Zhang).

http://dx.doi.org/10.1016/j.apcatb.2016.06.028
0926-3373/© 2016 Elsevier B.V. All rights reserved.

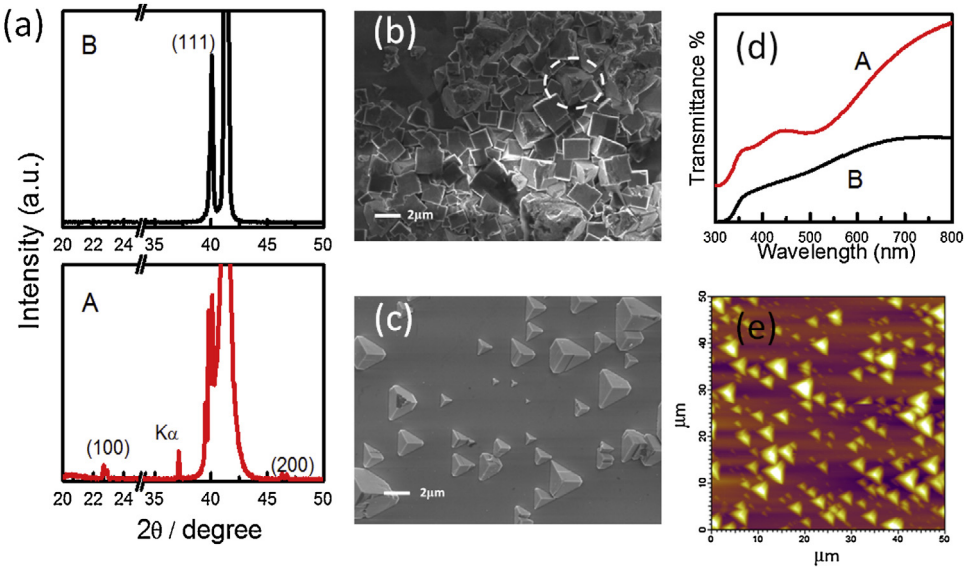


**Fig. 1.** (a) X-ray diffraction patterns, (b and c) top view SEM images of samples B and A, (d) UV–vis transmittance spectra and (e) AFM image of sample A. The dash circle in (b) marks the special morphology.

autoclave and submerged in the suspension. The hydrothermal reaction was performed in a drying oven at 180 °C for 3 h. After naturally cooling down to room temperature, we obtained the samples and rinsed the samples with de-ionized water and absolute ethyl alcohol to remove the residual unreacted precursor and unfixed $NaNbO_3$. For simplicity, hereafter the sample on $LaAlO_3(111)$ and $NaNbO_3/LaAlO_3(111)$ called A and B for short, respectively.

The crystal structures of prepared $NaNbO_3$ were identified by X-ray diffraction (XRD), and the morphology and microstructure of samples were observed using a scanning electron microscope (SEM) (JSM-7001F).

Photocatalytic activity for the decomposition of DCP and RhB in an aqueous solution was evaluated in the presence of samples A and B under full arc light irradiation of Xe lamp as reported previously [27,28]. The initial concentration of DCP and RhB solution was about 4.8 mg $L^{-1}$ and 2.5 mg $L^{-1}$. Before illumination, the reagent was left in the dark for 30 min to achieve adsorption-desorption equilibrium. The variation in the concentration of DCP and RhB was recorded by measuring the absorbance at 198 and 554 nm in the UV–vis spectrum (UV-2550, Shimadzu) every 10 min. In addition, photocatalytic degradation experiments with various scavengers were performed in order to detect the reactive species, and the process was similar to the original degradation experiment.

## 3. Results and discussion

The crystal structures and surface morphologies were different when the $NaNbO_3$ was grown on heterogeneous and homogeneous substrates, as shown in Fig. 1. The splitting double peaks, $(100)_c$ and $(200)_c$ peaks were obtained on sample A, indicating that the $NaNbO_3$ on sample A is polycrystalline with orthorhombic symmetry (JCPDS33-1270). However, when $LaAlO_3$ acts as a substrate in preparing $NaNbO_3$ by PLD, the single peak of $NaNbO_3$ would appear near the peak of substrate for each order [26], Interestingly, the adjacent diffraction peaks of $NaNbO_3$ and the substrate were observed in sample B, indicating that the $NaNbO_3$ prefers to grow along the $(111)_c$ of $NaNbO_3$ which is the same as the substrate. The surface morphologies were investigated by field-emission scanning electron microscopy (FESEM), as displayed in Fig. 1b and c. Some triangular pyramids were found on sample A, while the cubes on sample B. Furthermore, the element analysis confirms that triangular pyramids are $NaNbO_3$, and the blank is $LaAlO_3$ substrate. We found the typical triangular pyramid clearly in AFM image and the cross-section of FESEM image, as displayed in Figs. 1 e and 2 e, respectively. Usually, $NaNbO_3$ showed the nanowire or cube morphologies, when it was synthesized by the hydrothermal method without other inorganic or organic additions [29]. The morphologies of triangular pyramids were reported on $NaNbO_3$ grown on $SrTiO_3(111)$ single crystal substrate by PLD, while no such morphology was obtained when $LaAlO_3(111)$ is selected as the substrate [26,30].

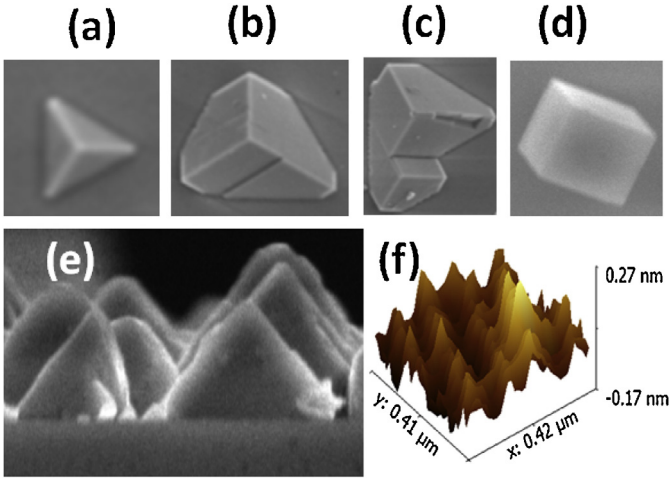


**Fig. 2.** (a–d) SEM images at different stages, (e) cross-section of SEM images of sample A and (f) AFM 3D image of the $LaAlO_3(111)$ after heating treatment.

The morphology was consistent with crystallography. All the samples grow along with the plane parallel to the substrate, and were terminated by {100}, which has the smallest surface free energy. When the sample was grown under the free growth condition, the {100} would be the preferred exposed facets. The growth stages of $NaNbO_3$ on $LaAlO_3(111)$ facet was proposed on the basis of different morphologies of sample, as shown in Fig. 2a–d. Moreover, we heated the $LaAlO_3(111)$ substrate at 1050 °C for 8 h, and found some nano-triangular pyramids, as shown in Fig. 2f. Therefore, we thought that the forming nuclei process should be induced by the

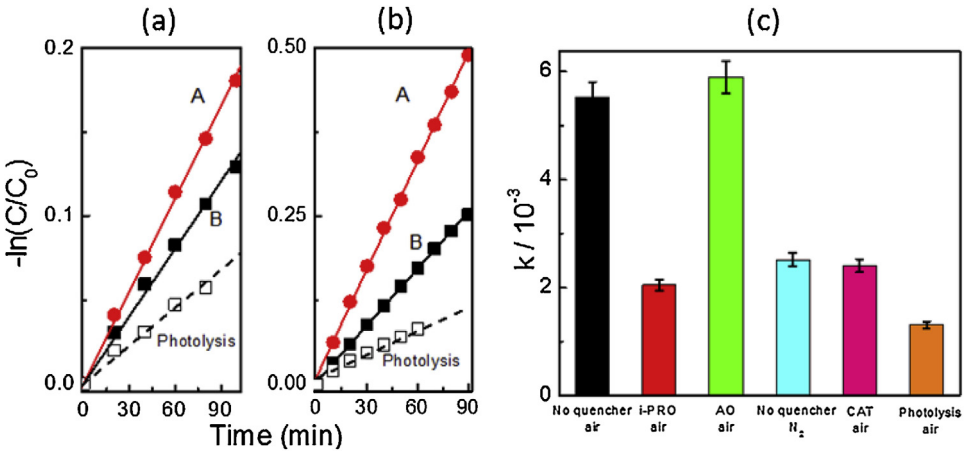


**Fig. 3.** Plot of $-\ln(C/C_0)$ vs. irradiation time for (a) DCP and (b) RhB in presence of samples A and B, and (c) the rate constants with various scavengers in presence of sample A under full arc irradiation of Xe lamp. Experimental conditions: *iso*-propanol (i-PRO): 10% at volume; ammonium oxalate (AO): 8.3 g/L; catalase (CAT): 0.5 g/L.

substrate of $LaAlO_3(111)$. Briefly, under the condition of hydrothermal process, raw material dissolved in hot water will adsorb on the surface of substrates and begin the process of nucleation on the surface. Then the small triangular pyramids terminated with three right triangles distribute themselves across the flat $LaAlO_3(111)$. Then the triangular pyramid's basic angles look like being truncated and the dislocation lines appear on the sides when it further grows up. We observed that two truncated triangular pyramids will weld themselves together when they encountered. The truncated triangular pyramid will become a cube with one truncated tip while it stands there. In other words, the cube with one truncated tip is at a stable state when the center of gravity is over the bottom side. Moreover, the triangular pyramid with the truncated top angle was observed when it becomes too large as marked in Fig. 1b with dash cycle.

Based on above crystal growth mechanism, we considered the difference in morphology coming from the growth rate, which on the homogeneous substrate is faster than that on the heterogeneous substrate due to the better lattice match. At the initial stage of crystallization, the $NaNbO_3$ will epitaxial grow on the nano-triangular pyramids of $LaAlO_3$. The triangular pyramids would appear on the substrate, as shown in Fig. 1c. We also found the bigger triangular pyramids under the cubes on the sample B, as marked in Fig. 1b with dash cycle, indicating that the morphologies of sample would be triangular pyramids firstly. The cube is grown on the {100} facets. Moreover, another indirect support is that the cubes are observed when we used $LaAlO_3(100)$ as substrate under the same condition (not shown here).

The sample A (triangle pyramids) shows the higher activity than sample B (cubes). When the reagent solution is dilute, the reaction rate ($r$) can be expressed as $r = kC$, where, $k$ is the apparent rate constant, and $C$ is the instantaneous concentration of the reactant. The plots of $-\ln(C/C_0)$ vs. time were shown in Fig. 3a and b. DCP is a colorless organic pollutant and no self-sensitive degradation during estimating the photocatalytic activity. The $k$ of samples A and B for DCP degradation is $1.84 \times 10^{-3}$ min$^{-1}$ and $1.34 \times 10^{-3}$ min$^{-1}$, which is about twice that of photolysis, indicating that both samples exhibit the abilities of photocatalytic oxidization. The photocatalytic activities of RhB degradation were also displayed, the $k$ of sample A is $5.53 \times 10^{-3}$ min$^{-1}$, which is nearly two times higher in comparison with that of sample B of $2.87 \times 10^{-3}$ min$^{-1}$. Photocatalytic activity could be affected by many factors, such as the mass of catalyst, absorption property, morphology and so on. For our samples, sample B has more $NaNbO_3$ than sample A judging from the cross-section SEM images (not shown here). For the absorption property, they have the same absorption edge, as displayed in Fig. 1d, and we did not add any dopant in the sample. Consequently, we could not attribute the different activity to the light absorption. The two samples show the quite different morphologies. Therefore, the different morphology was considered as the main reason causing the different photoactivity, although the detailed mechanism how the morphology affects the activity is not clear yet.

It is well known that the generation of electron-hole pairs is the beginning of photocatalytic oxidization process. Subsequently, a series of reactive oxygen species, such as $^{\bullet}OH$, $H_2O_2$ and $^{\bullet}O_2^-$, are formed during the reaction and directly influence the properties of photocatalytic activity. In order to elucidate the photocatalytic oxidization process, the control experiments were carried out by using several kinds of scavengers. The effects of different scavengers on $k$ of RhB degradation over sample A was shown in Fig. 3c [31,32]. The more $k$ is reduced when the more important role the oxidizing species plays in the reaction. When the $h^+$ scavenger, ammonium oxalate (AO), was added into the reagent solution, the degradation of RhB was not suppressed. The k even had a slight increase from $5.5 \times 10^{-3}$ to $5.9 \times 10^{-3}$ min$^{-1}$, which confirmed that $h^+$ is not the main reactive species. In contrast, the $k$ decreased obviously to $2.05 \times 10^{-3}$ min$^{-1}$, almost the same as that of photolysis when the $^{\bullet}OH$ scavenger, isopropanol (i-PrOH), was added, revealing that $^{\bullet}OH$ is the predominant reactive species involved in reaction. The contribution of $H_2O_2$ in reaction was investigated by using catalase (CAT). The corresponding rate constant $k$ was $2.4 \times 10^{-3}$ min$^{-1}$, which suggests that $H_2O_2$ is also an important reactive species in the photocatalytic oxidization process. The generation of superoxide radicals $^{\bullet}O_2^-$ could be via photoinduced electrons reacting directly with $O_2$ adsorbed on the surface of the catalyst. As shown in Fig. 3c, the $k$ decreased to $2.5 \times 10^{-3}$ min$^{-1}$ under the anoxic suspension ($N_2$-saturated condition), indicating that $O_2$ is to primarily act as an efficient electron trap, leading to the generation of $^{\bullet}O_2^-$ and preventing the recombination of electrons and holes.

Based on the consequence of radical scavenger experiments, the possible degradation mechanism on sample A was proposed and illustrated as in Fig. 4. The photocatalytic processes can be described as follows:

$$NaNbO_3 + h\nu \rightarrow NaNbO_3(e_{CB}^- + h_{VB}^+)$$

$$e_{CB}^- + O_2 \rightarrow O_2^{\bullet -}$$

$$O_2^{\bullet -} + H^+ \rightarrow HO_2^{\bullet}$$

$$HO_2^{\bullet} + O_2^{\bullet -} + H^+ \rightarrow O_2 + H_2O_2$$

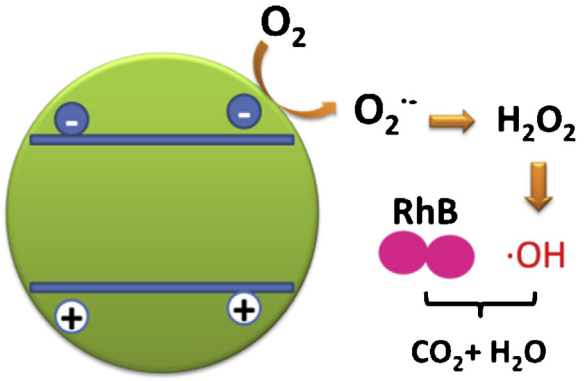


**Fig. 4.** Schematic of the possible reaction mechanism over sample A under full arc irradiation of Xe lamp.

$$H_2O_2 + e^-_{CB} \rightarrow OH^- + HO^{\bullet}$$

$$HO^{\bullet} + RhB \rightarrow products$$

When $NaNbO_3$ films are excited under full arc irradiation of Xe lamp, the photogenerated electron-hole pairs could be produced in their conduction and valence band. After that, electrons rapidly react with adsorbed $O_2$ on the surface of films to generate $^{\bullet}O_2^-$, realize the efficient charge separation and further convert into other reactive species such as $H_2O_2$. The degradation by direct oxidation of $H_2O_2$ is negligible due to its low reaction rate, therefore, the role of $H_2O_2$ is to generate $^{\bullet}OH$ radicals via decomposition. There is no doubt that the suppression of any intermediate steps, for instance, the deficiency of oxygen or the capture of $H_2O_2$ and $^{\bullet}OH$ radicals will cause the decline of the photocatalytic activity. As seen from the quenching results, $h^+$, which is one effective oxidative active species to many toxic organic pollutants, is almost no contribution to the photodegradation procedure over sample A. The slightly increase of $k$ when AO added is possibly caused by the reduction of carrier recombination due to the capture of $h^+$.

## 4. Conclusions

In summary, the $NaNbO_3$ with the morphologies of triangular pyramid and cube are obtained on the heterogeneous and homogeneous substrate due to different growth rate. They show the abilities of photocatalytic oxidization for DCP and RhB. The $^{\bullet}OH$ radicals coming from $^{\bullet}O_2^-$ with the intermediate of $H_2O_2$ was the dominant oxide species. The reported method will be used to improve the photocatalytic activity via forming special morphology.

## Acknowledgements

This work was supported by the Young Core Instructor Foundation from the Education Commission of Henan Province (2015GGJS-021), the National Natural Science Foundation of China (51402088), 863 Program of China (2015AA034201), the Program for Science & Technology Innovation Talents in Universities of Henan Province, China (17HASTIT014), and the Open Research Fund of Jiangsu Provincial Key Laboratory for Nanotechnology (Nanjing University).

## References

[1] H. Kisch, Angew. Chem. Int. Ed. 52 (2013) 812–847.
[2] H. Han, C. Li, Natl. Sci. Rev. 2 (2015) 146–147.
[3] F.E. Osterloh, Chem. Soc. Rev. 42 (2013) 2294–2320.
[4] S. Cao, J. Low, J. Yu, M. Jaroniec, Adv. Mater. 27 (2015) 2150–2176.
[5] H. Wang, L. Zhang, Z. Chen, J. Hu, S. Li, Z. Wang, J. Liu, X. Wang, Chem. Soc. Rev. 43 (2014) 5234–5244.
[6] T. Hisatomi, J. Kubota, K. Domen, Chem. Soc. Rev. 43 (2014) 7520–7535.
[7] S. Bin Anooz, P. Petrik, M. Schmidbauer, T. Remmele, J. Schwarzkopf, J. Phys. D: Appl. Phys. 48 (2015) 385303.
[8] J. Schwarzkopf, D. Braun, M. Schmidbauer, A. Duk, R. Wordenweber, J. Appl. Phys. 115 (2014).
[9] B. Zielinska, J. Srenscek-Nazzal, R.J. Kalenczuk, Pol. J. Chem. Technol. 10 (2008) 1–3.
[10] K. Katsumata, C.E.J. Cordonier, T. Shichi, A. Fujishima, J. Am. Chem. Soc. 131 (2009) 3856–3857.
[11] K. Saito, A. Kudo, Inorg. Chem. 49 (2010) 2017–2019.
[12] H.F. Shi, T.Z. Wang, J. Chen, C. Zhu, J.H. Ye, Z.G. Zou, Catal. Lett. 141 (2011) 525–530.
[13] S.F. Chen, L. Ji, W.M. Tang, X.L. Fu, Dalton Trans. 42 (2013) 10759–10768.
[14] X.K. Li, Q. Li, L.Y. Wang, Phys. Chem. Chem. Phys. 15 (2013) 14282–14289.
[15] L.Q. Jiang, Y.H. Zhang, Y. Qiu, Z.G. Yi, RSC Adv. 4 (2014) 3165–3170.
[16] P. Li, H. Xu, L.Q. Liu, T. Kako, N. Umezawa, H. Abe, J.H. Ye, J. Mater. Chem. 2 (2014) 5606–5609.
[17] G.Q. Li, T. Kako, D.F. Wang, Z.G. Zou, J. Ye, J. Solid State Chem. 180 (2007) 2845–2850.
[18] H. Xu, C.T. Liu, H.M. Li, Y.G. Xu, J.X. Xia, S. Yin, L. Liu, X.Y. Wu, J. Alloy. Compd. 509 (2011) 9157–9163.
[19] J.W. Liu, G. Chen, Z.H. Li, Z.G. Zhang, Int. J. Hydrogen Energy 32 (2007) 2269–2272.
[20] H.F. Shi, X.K. Li, D.F. Wang, Y.P. Yuan, Z.G. Zou, J.H. Ye, Catal. Lett. 132 (2009) 205–212.
[21] X.B. Li, G.Q. Li, S.J. Wu, X.R. Chen, W.F. Zhang, J. Phys. Chem. Solids 75 (2014) 491–494.
[22] K.J. Zhu, Y. Cao, X.H. Wang, L. Bai, J.H. Qiu, H.L. Ji, CrystEngComm 14 (2012) 411–416.
[23] M. Faisal, A.A. Ibrahim, H. Bouzid, S.A. Al-Sayari, M.S. Al-Assiri, A.A. Ismail, J. Mol. Catal. A: Chem. 387 (2014) 69–75.
[24] S. Kim, J.H. Lee, J. Lee, S.W. Kim, M.H. Kim, S. Park, H. Chung, Y.I. Kim, W. Kim, J. Am. Chem. Soc. 135 (2013) 6–9.
[25] W.L. Suchanek, Chem. Mater. 16 (2004) 1083–1090.
[26] G.Q. Li, Z.G. Yi, Y. Bai, W.F. Zhang, H.T. Zhang, Dalton Trans. 41 (2012) 10194–10198.
[27] G.Q. Li, Z.G. Yi, H.T. Wang, C.H. Jia, W.F. Zhang, Appl. Catal. B: Environ. 158–159 (2014) 280–285.
[28] G. Li, T. Varga, P. Yan, Z. Wang, C. Wang, S.A. Chambers, Y. Du, Phys. Chem. Chem. Phys. 17 (2015) 15073–15462.
[29] H.Y. Zhu, Z.F. Zheng, X.P. Gao, Y.N. Huang, Z.M. Yan, J. Zou, H.M. Yin, Q.D. Zou, S.H. Kable, J.C. Zhao, Y.F. Xi, W.N. Martens, R.L. Frost, J. Am. Chem. Soc. 128 (2006) 2373–2384.
[30] S. Yamazoe, H. Sakurai, M. Fukada, H. Adachi, T. Wada, Appl. Phys. Lett. 95 (2009) 062906.
[31] Y. Park, Y. Na, D. Pradhan, B.-K. Min, Y. Sohn, CrystEngComm 16 (2014) 3155.
[32] J. Cao, B.D. Luo, H.L. Lin, B.Y. Xu, S.F. Chen, Appl. Catal. B: Environ. 111 (2012) 288–296.